Lgl resets Par complex membrane loading at mitotic exit to enable asymmetric neural stem cell division

Bryce LaFoya*, Sarah E. Welch*, and Kenneth E. Prehoda[1]

Institute of Molecular Biology
Department of Chemistry and Biochemistry
1229 University of Oregon
Eugene, OR 97403

*contributed equally

[1]Corresponding author: prehoda@uoregon.edu

Summary

The Par complex regulates cell polarity in diverse animal cells[1–4], but how its localization is restricted to a specific membrane domain remains unclear. We investigated how the tumor suppressor Lethal giant larvae (Lgl) polarizes the Par complex in *Drosophila* neural stem cells (NSCs or neuroblasts). In contrast to epithelial cells, where Lgl and the Par complex occupy mutually exclusive membrane domains, Lgl is cytoplasmic when the Par complex is apically polarized in NSCs[5]. Importantly, we found that Lgl's key function is not in directly regulating metaphase Par polarity, but rather in removing the Par complex from the membrane at the end of mitosis, creating a "polarity reset" for the next cell cycle. Without this Lgl-mediated reset, we found that residual Par complex remains on the basal membrane during subsequent divisions, disrupting fate determinant polarization and proper asymmetric cell division. These findings reveal a novel mechanism of polarity regulation by Lgl and highlight the importance of the pre-polarized state in Par-mediated polarity.

Introduction

Cortical polarity is a fundamental cellular characteristic that underlies diverse biological processes, including directional cell migration, tissue organization, and asymmetric cell division. The Par complex, consisting of Par-6 and atypical Protein Kinase C (aPKC), plays a pivotal role in establishing and maintaining polarity in a wide range of animal cells, from epithelial cells to neurons[1–3,6]. The proper localization and function of the Par complex are particularly critical in stem cells, where asymmetric distribution of cell fate determinants governs the delicate balance between self-renewal and differentiation. A fundamental question in cell polarity research is how the Par complex itself is restricted to specific membrane domains. The tumor suppressor Lethal giant larvae (Lgl) plays a key role in Par polarity by restricting the Par complex to the proper membrane domain[5,7–10], but how Lgl controls Par complex localization remains an open question.

Par polarity is the result of a complex interplay of positive and negative regulators. While factors like Par-3 (Bazooka in *Drosophila*) and Cdc42 ensure that the Par complex is targeted to the membrane[11–13], the negative regulation provided by Lgl restricts the complex to a specific membrane domain. Lgl is thought to perform this critical function by mutual exclusion: the Par complex and Lgl reciprocally control one another's localization by binding to the membrane[3,5,7,14]. The mutual exclusion model is exemplified by interphase epithelial cells,

33 where the Par complex is confined to the apical plasma membrane while Lgl occupies the
34 basolateral domain (Fig. 1A). Loss of either component, Lgl or Par complex, allows the other to
35 enter the incorrect domain[5,7,9]. How the Par complex excludes Lgl from the Par domain is well-
36 understood[15–17], but little is known about how Lgl regulates Par complex localization.

37 Like epithelial cells, proper Par localization in NSCs requires Lgl[4,12,18,19]. In NSCs lacking Lgl
38 function, the Par complex is localized across the entire membrane instead of being restricted
39 to its proper domain[12,18], similar to epithelia. However, a key difference between Lgl's behavior
40 in NSCs and epithelia lies in Lgl's localization. Instead of localizing to a complementary
41 membrane domain, Lgl is cytoplasmic when the Par complex is polarized in NSCs[5] (Fig. 1A).
42 Polarized Par complex with cytoplasmic Lgl has also been observed in sensory organ
43 precursor (SOP) cells[20], further challenging the exclusion model. Thus, Lgl's behavior in NSCs
44 and SOPs indicates that Lgl can regulate Par complex localization without being on the
45 membrane.

46 **Results and Discussion**

47 **Patterned Lgl membrane dynamics during NSC mitosis**

48 To gain insight into how Lgl regulates Par complex localization in NSCs, we first examined
49 Lgl's membrane localization dynamics including how it is restored to the membrane following
50 mitosis. We imaged Lgl's localization in NSCs from *Drosophila* larval brain explants expressing
51 Lgl-GFP (expressed by Worniu-GAL4 driven UAS) and Histone H2A-RFP (expressed from its
52 endogenous locus) using rapid, super-resolution spinning disk confocal microscopy (Fig. 1B).
53 Lgl removal from the membrane began in early prophase, initiating at a small area near the
54 apical pole of the cell and spreading rapidly across the membrane such that it appeared to be
55 completely removed by late prophase (Fig. 1C,D; Video 1). This pattern could be observed
56 both in medial sections and maximum intensity projections of the full cell volume (Fig. 1E;
57 Video 1). The full volume data also revealed how Lgl displacement from the membrane was
58 affected by the membrane structures that are present on the NSC surface[21–23]. Lgl was
59 enriched in the membrane structures, consistent with their higher membrane density. Lgl
60 disappeared from the structures as it was displaced from the membrane, while the structures
61 themselves remained evident when imaging a membrane sensor (Video 1).

62 While Lgl appeared to be completely removed from the membrane when imaging NSCs in
63 intact tissue, progeny cells adhered to the basal region prevented a definite determination. We

64 imaged individual cultured NSCs that had been dissociated from brains to observe basal Lgl
65 dynamics in the absence of adhering cells. The Lgl dynamics in dissociated NSCs were
66 consistent with our initial observations of apically-directed membrane clearing and provided
67 unambiguous evidence that Lgl is indeed completely removed from the membrane by late
68 prophase (Fig. 1F,G; Video 1). The patterned Lgl membrane displacement dynamics indicate
69 that removal is a spatially regulated process, like that observed for SOPs[20], rather than one in
70 which it is simultaneously removed from the membrane.

71 NSCs undergo repeated cycles of asymmetric division such that Lgl must be restored to the
72 membrane at some point to achieve its interphase localization state. We analyzed Lgl
73 dynamics in both intact brain and dissociated NSCs to determine when and how Lgl is
74 restored to the membrane following mitosis. Our results showed that Lgl becomes rapidly
75 restored to the membrane at the completion of mitosis, beginning near the cytokinetic pore
76 connecting the nascent sibling cells (Fig. 1H-J; Videos 1,3), similar to the dynamics observed in
77 follicular epithelial cells[24]. Our results provide a detailed description of Lgl's dynamic
78 localization throughout the cell cycle in NSCs, revealing precise spatial and temporal control of
79 its membrane association (Fig. 1K).

80 **aPKC removes Lgl from the NSC early in mitosis**

81 Since Lgl is cytoplasmic at metaphase in NSCs, when the Par complex is polarized, we sought
82 to understand how it transitions between membrane-bound and cytoplasmic states. Evidence
83 from various cell types indicates that Lgl can be phosphorylated and removed from the
84 membrane by the Par complex subunit atypical Protein Kinase C (aPKC) but also by the mitotic
85 kinase Aurora A[5,7]. Aurora A could also regulate Lgl's membrane association indirectly by
86 influencing aPKC polarity[20,25]. We sought to determine whether one or both kinases are
87 responsible for the patterned removal of Lgl from the NSC membrane during prophase. To
88 dissect the relative contributions of aPKC and Aurora A to Lgl removal, we separately inhibited
89 aPKC or Aurora A activity and assessed the effect on Lgl localization dynamics. We inhibited
90 aPKC by expressing a UAS-controlled aPKC RNAi specifically in larval brain NSCs using
91 Worniu-GAL4 driven expression. For Aurora A inhibition, we added the specific inhibitor
92 MLN8237[7] to the larval brain explant culture media.

93 In NSCs where aPKC was depleted by RNAi, we observed that Lgl removal from the
94 membrane in mitosis was largely inhibited (Fig. 2A,B; Video 2). Unlike wild-type NSCs, where

95 Lgl was removed from the membrane late in prophase, aPKC RNAi NSCs had persistent Lgl
96 membrane enrichment throughout mitosis. We did detect a small decrease in apical Lgl
97 membrane signal beginning in early prophase (Fig. 2A,B) suggesting the presence of residual
98 aPKC activity or a small contribution from another mechanism. The retention of Lgl on the
99 membrane in aPKC-depleted cells indicates that aPKC-mediated phosphorylation is the
100 primary mechanism driving Lgl dissociation from the plasma membrane as NSCs enter mitosis.
101 Interestingly, Lgl's membrane enrichment during interphase was enhanced in aPKC RNAi
102 NSCs (Fig. 2A,B), suggesting that Lgl exchanges between the membrane and cytoplasm due
103 to phosphorylation and dephosphorylation in wild-type NSCs.

104 We also tested if Aurora A activity is required for Lgl membrane displacement as it can directly
105 phosphorylate Lgl and can also regulate aPKC polarity[5,7,20,25]. Consistent with our results
106 indicating that aPKC is the dominant kinase responsible for displacement of Lgl from the
107 membrane in NSCs, we found that inhibition of Aurora A activity with MLN8237 did not cause a
108 significant difference in Lgl removal from the membrane compared to wild-type NSCs (Fig.
109 2C,D; Video 2). The patterned removal of Lgl from the membrane proceeded with similar
110 dynamics and extent as observed in untreated cells. However, we did observe cytokinesis
111 defects in treated NSCs (Fig. 2C; Video 2) indicating that Aurora A was successfully inhibited.
112 We conclude that, despite its known ability to phosphorylate Lgl, Aurora A does not participate
113 in the removal of Lgl from the NSC membrane. This conclusion is consistent with a previous
114 study demonstrating that Aurora A phosphorylation sites on Lgl aren't required for NSC
115 membrane displacement[5].

116 **Correlated aPKC and Lgl membrane dynamics**

117 We next sought to determine the degree to which aPKC and Lgl membrane dynamics are
118 spatially and temporally correlated. The recruitment of aPKC to the membrane in early
119 prophase is a complex, multistep process where aPKC is initially localized to small domains on
120 the apical membrane before coalescing into an apical cap by metaphase[26,27]. To determine the
121 interplay between Lgl's disappearance and aPKC's appearance on the membrane, we
122 simultaneously imaged aPKC-GFP (expressed from its endogenous promoter) and Lgl-
123 mCherry (expressed by Worniu-GAL4 driven UAS) in NSCs. This approach allowed us to
124 directly observe the spatial and temporal dynamics of aPKC recruitment with the pattern of Lgl
125 removal from the cell membrane. Lgl removal at the apical pole of the NSC was tightly
126 correlated with the appearance of aPKC at that site (Fig. 3A-C; Video 3). In the apical

127 hemisphere, the appearance of aPKC at the membrane was strongly correlated with Lgl
128 removal. However, Lgl was also removed from the basal membrane even though aPKC does
129 not localize there. We conclude that aPKC removes Lgl from the membrane both directly (i.e.
130 apical membrane) and indirectly (i.e. basal membrane). Indirect removal of basal Lgl by apical
131 aPKC is likely influenced by factors such as the rate of Lgl diffusion along the plasma
132 membrane.

133 Near the end of mitosis, aPKC spread along the nascent NSC membrane while being excluded
134 from the membrane of the smaller nascent neural precursor (NP)[26] (Figure 3D; Video 3). Shortly
135 after it reached the furrow, aPKC was removed from the membrane. We observed patterned
136 removal of aPKC from the membrane that was correlated with Lgl's membrane reloading at
137 mitotic exit (Figs. 1H,I, 3D-F; Video 3). As Lgl accumulated on the basal membrane of the
138 nascent NSC near the cytokinetic pore, aPKC was removed from the membrane in a
139 complementary pattern. Lgl continued to spread along the membrane until it occupied both
140 basal and apical membrane and aPKC was no longer detectable on the membrane (Fig. 3D-F).

141 **Lgl excludes basal aPKC by regulating its interphase membrane association**

142 The mutual exclusion model, which posits that Lgl and the Par complex reciprocally control
143 each other's localization by occupying opposing membrane domains, does not explain the
144 behavior of these proteins in SOPs[20] or NSCs[5] (Fig. 3A). The primary inconsistency is the
145 metaphase polarized state when the Par complex is polarized while Lgl is cytoplasmic.
146 However, it is also not known whether Lgl is responsible for excluding aPKC from the
147 membrane during interphase in NSCs. To gain insight into how Lgl regulates Par complex
148 localization in these contexts, we examined aPKC localization in NSCs expressing Lgl RNAi
149 (Worniu-GAL4 driven UAS). While aPKC is excluded from the cell membrane during interphase
150 in wild-type NSCs, aPKC was not removed from the membrane at the end of mitosis in Lgl
151 RNAi NSCs, remaining on the membrane throughout interphase and the subsequent mitosis
152 (Fig. 4A-D; Video 4). However, the accumulation of aPKC at the apical membrane during early
153 mitosis did not require Lgl, occurring both in wild-type and Lgl RNAi NSCs (Fig. 4A,C; Video 4).
154 Apical enrichment caused aPKC to be polarized in both contexts at metaphase (Fig. 4E), with
155 the key difference that Lgl RNAi NSCs had detectable basal aPKC at this stage (Fig. 4D). We
156 conclude that Lgl is required to remove aPKC from the membrane at mitotic exit in NSCs but is
157 not required for apical enrichment of the Par complex during early mitosis.

158 **Lgl resets Par polarity for subsequent asymmetric NSC division**

159 Our results provide a more nuanced view of Lgl function in Par polarity than provided by the
160 mutual exclusion model. Rather than directly regulating metaphase Par polarity by occupying
161 an opposing membrane domain, Lgl acts much earlier in the cell cycle to clear the Par complex
162 from the NSC membrane at the end of mitosis. This mechanism ensures that each cell cycle
163 begins without Par complex on the membrane (Fig. 4F). The importance of this "polarity reset"
164 can be seen in NSCs where the Par complex isn't removed from the membrane. In NSCs
165 lacking Lgl function, the Par complex remains on the membrane after mitosis. Shortly after
166 mitotic entry, the Par complex becomes enriched at the apical membrane, like in wild-type
167 NSCs (Fig. 4C,E). However, residual basal Par complex from interphase (Fig. 4D) prevents fate
168 determinant polarization[18], disrupting asymmetric cell division. Thus, Lgl is not required for Par
169 polarity in NSCs but instead ensures the Par complex is removed from the membrane when
170 polarization begins in early mitosis. In other words, Par polarity is insufficient to support NSC
171 asymmetric division – the Par complex must be on the apical membrane and not on the basal
172 membrane. Basal Par complex, even at the reduced levels we observed compared to apically-
173 enriched complex, disrupts fate determinant polarity and asymmetric cell division[18].

174 While the metaphase polarized state has long been the focus of NSC asymmetric cell division
175 research[2,28–31], our results highlight the importance of the progression from mitosis to
176 interphase to the process. Asymmetric cell division couples transitions in cell fate to the
177 division cycle and fate transitions likely occur at or near mitotic exit. Consistent with the
178 importance of this cell cycle phase, fate determinants are activated shortly after the end of
179 mitosis[32]. The midbody that forms in the intercellular bridge connecting nascent siblings plays
180 a key role in mediating asymmetric fate specification[32]. Intriguingly, Lgl membrane reloading
181 and the concomitant displacement of aPKC into to the cytoplasm begins at or near the
182 midbody (Fig. 3D-F) suggesting that fate specification and resetting polarity could be regulated
183 by the same pathways.

184 The mechanism by which Lgl removes aPKC from the membrane at the end of mitosis remains
185 an intriguing question. There are several possibilities based on our current understanding of Lgl
186 and aPKC. One potential mechanism is that Lgl, upon its rapid return to the membrane post-
187 mitosis, could act as a competitive inhibitor for aPKC membrane binding sites. Lgl's strong
188 affinity for the membrane[15,16] might allow it to outcompete aPKC and displace it from the
189 membrane. Alternatively, Lgl could recruit or activate a phosphatase that dephosphorylates

190 aPKC or its binding partners, thereby reducing aPKC's affinity for the membrane. Further
191 investigation into these potential mechanisms will be crucial for fully understanding Lgl's role in
192 polarity regulation.

193 **Figure Legends**

194 Figure 1 Patterned Lgl displacement and reloading during neural stem cell asymmetric division
195 (A) Mutual exclusion model for Par polarity. In this model, the Par complex (comprised of Par-6
196 and atypical Protein Kinase C or aPKC) establishes a mutually exclusive membrane domain
197 with Lethal giant larvae (Lgl), wherein the presence of one protein on the membrane prevents
198 the binding of the other. This model is consistent with the localization pattern in epithelial cells
199 but not Drosophila neural stem cells (NSCs) and sensory organ precursors, where the Par
200 complex becomes polarized during mitosis while Lgl remains cytoplasmic.
201 (B) Imaging Drosophila larval brain neural stem cells (NSCs). The larval central nervous system
202 (CNS), including the brain lobes and ventral nerve cord, was extracted from third-instar larvae
203 (L3). Neural stem cells (NSCs), characterized by their relatively large size, specific locations
204 within the brain, and expression of tissue-specific transgenes, were either imaged within the
205 intact CNS or, alternatively, the tissue was dissociated to isolate and image the NSCs
206 individually.
207 (C) Removal of Lgl from the plasma membrane in early mitosis in an NSC from the intact CNS.
208 Frames from Video 1 are shown. The NSC (marked with asterisk) is expressing Lgl-GFP
209 (expressed from Worniu-GAL4 driven UAS) and Histone H2A (His2a-RFP). Time is shown
210 relative to anaphase onset.
211 (D) Patterned removal of Lgl from the plasma membrane in early mitosis. The ratio of
212 membrane-to-cytoplasmic Lgl is presented for ten distinct neural stem cells (NSCs) in the
213 apical and lateral regions during early mitosis, when Lgl was first cleared from the apical
214 membrane. The Gardner-Altman estimation plot illustrates the paired measurements for each
215 NSC. Additionally, the 95% confidence interval is displayed in the mean difference
216 comparison, along with the corresponding bootstrap distribution from which it was derived.
217 (E) A 3D projection of Lgl dynamics during early mitosis. Frames from Video 1 are shown. The
218 NSC is expressing Lgl-GFP (expressed from Worniu-GAL4 driven UAS). The top row depicts a
219 medial optical section. The bottom row depicts a maximum intensity projection (MIP) of optical
220 sections across one hemisphere of the cell. Time is shown relative to anaphase onset.

221 (F) Removal of Lgl from the plasma membrane in early mitosis in an NSC dissociated from the
222 CNS. Frames from Video 1 are shown. The NSC is expressing Lgl-GFP (expressed from
223 Worniu-GAL4 driven UAS) and Histone H2A (His2a-RFP). Time is shown relative to anaphase
224 onset.
225 (G) The timing of the clearance of the basal Lgl membrane signal, represented by a membrane-
226 to-cytoplasmic signal ratio close to one, is presented for three dissociated neural stem cells
227 (NSCs) in relation to metaphase.
228 (H) Lgl reloading to the plasma membrane in early interphase in an NSC from an intact CNS.
229 Frames from Video 1 are shown as in (C). Time is shown relative to anaphase onset.
230 (I) Lgl reloading to the plasma membrane in early interphase in an NSC dissociated from the
231 CNS. Frames from Video 1 are shown as in (F).
232 (J) Lgl patterned membrane reloading in early interphase. The ratio of membrane-to-
233 cytoplasmic Lgl is shown for two time points: one at the conclusion of anaphase and another
234 during interphase. Measurements were taken near the cytokinetic midbody as well as along the
235 lateral and apical membranes.
236 (K) Schematic representation of Lgl membrane dynamics in neural stem cells (NSCs). During
237 interphase, Lgl is distributed across the NSC membrane. In early mitosis, membrane clearing
238 begins starting at the apical pole and fully clearing by prophase. Membrane reloading of Lgl
239 begins in early interphase beginning near the midbody region.
240 Figure 2 aPKC but not Aurora A is required for Lgl removal from the NSC membrane in early
241 mitosis
242 (A) Lgl dynamics in an NSC from the intact central nervous system expressing aPKC RNAi.
243 Frames from Video 2 are shown. The NSC is expressing Lgl-GFP and aPKC RNAi (both
244 expressed from Worniu-GAL4 driven UAS). Time is shown relative to anaphase onset. The
245 same timepoints are shown from an NSC expressing Lgl-GFP, but not expressing aPKC RNAi
246 for a wild-type (”WT”) comparison.
247 (B) aPKC is required for Lgl removal from the membrane in early mitosis. The Gardner-Altman
248 estimation plot displays error bars indicating one standard deviation (with the gap representing
249 the mean). The bar in the mean difference comparison reflects the bootstrap 95% confidence
250 interval. Each data point corresponds to a measurement taken from a distinct NSC.
251 (C) Lgl dynamics in an NSC from the intact central nervous system incubated with the specific
252 Aurora A inhibitor MLN8237. Frames from Video 2 are shown. The NSC is expressing Lgl-GFP
253 along with aPKC RNAi, both driven by Worniu-GAL4 and UAS. Arrowheads indicate furrow

254 retraction during late cytokinesis, providing evidence of drug effectiveness. The time is shown
255 relative to anaphase onset. For comparison, similar timepoints are depicted for an NSC
256 incubated with DMSO alone (vehicle control).
257 (D) Aurora A inhibition does not detectabley influence Lgl membrane displacement in early
258 mitosis. Lgl apical membrane-to-cytoplasmic ration is shown for reated with either MLN8237 or
259 the vehicle control (DMSO) during interphase, prophase, and metaphase. The Gardner-Altman
260 estimation plot displays error bars representing one standard deviation (with the gap indicating
261 the mean). The bar representing the mean difference comparison reflects the bootstrap 95%
262 confidence interval.
263 Figure 3 Correlated aPKC and Lgl NSC membrane dynamics
264 (A) Lgl and aPKC dynamics in an NSC from the intact central nervous system (CNS) during Lgl
265 membrane clearance at mitotic entry. Frames from Video 3 are shown. The NSC is expressing
266 aPKC-GFP (expressed from its native promoter) and Lgl-mCherry (expressed from Worniu-
267 GAL4 driven UAS). Time is indicated relative to anaphase onset.
268 (B) Lgl patterned removal at mitotic entry. The membrane-to-cytoplasmic ratio of Lgl was
269 assessed both before and during the clearance of Lgl from the membrane, specifically at the
270 apical and lateral membrane. The Gardner-Altman estimation plot displays error bars that
271 indicate one standard deviation, with the gap denoting the mean value. The bar in the mean
272 difference comparison illustrates the bootstrap 95% confidence interval. Each point on the plot
273 corresponds to a measurement taken from a distinct NSC. Time is indicated relative to
274 anaphase onset.
275 (C) aPKC is apically enriched when Lgl begins clearing from the membrane at mitotic entry. The
276 membrane-to-cytoplasmic ratio of aPKC is presented both before and during the clearance of
277 Lgl from the membrane, measured at the apical and lateral membrane. Plotted as in (B)
278 (D) The dynamics of Lgl and aPKC in an NSC from the intact CNS during the clearance of
279 aPKC from the membrane at mitotic exit are illustrated with frames extracted from Video 3. The
280 NSC is expressing aPKC-GFP driven by its native promoter and Lgl-mCherry expressed by
281 Worniu-GAL4 driven UAS. Time is indicated relative to the beginning of the imaging session.
282 (E) Lgl patterned membrane reloading at mitotic exit. At mitotic exit, as aPKC begins to clear
283 from the membrane, Lgl is basally enriched at the site where the cytokinetic furrow reorganizes
284 into the midbody. The ratio of membrane-to-cytoplasmic Lgl is presented both before and
285 during the clearing of aPKC from the membrane, measured at the lateral membrane and near
286 the furrow (as the midbody forms). The data is plotted as shown in panel (B).

287 (F) aPKC patterned removal at mitotic exit. The ratio of membrane-to-cytoplasmic aPKC is
288 presented both before and during the clearing of aPKC from the membrane, measured at the
289 lateral membrane and near the furrow (as the midbody forms). The data is plotted as shown in
290 panel (B)
291 Figure 4 Lgl resets NSC polarity by removing aPKC from the membrane at mitotic exit
292 (A) aPKC dynamics in an NSC from the intact central nervous system expressing Lgl RNAi. The
293 frames from Video 4 are presented, showcasing an NSC expressing aPKC-GFP, driven by its
294 native promoter, and Lgl RNAi, induced by Worniu-GAL4 driving UAS. Arrowheads indicate the
295 presence of basal aPKC before and during mitosis. Time is indicated relative to the onset of
296 anaphase. For comparison, an NSC that does not express Lgl RNAi (wild-type "WT") is shown
297 at corresponding time points.
298 (B) Lgl is required to remove aPKC from the membrane during the return to interphase. A
299 comparison of apical aPKC membrane enrichment in NSCs both expressing and not
300 expressing Lgl RNAi during interphase, prophase, and metaphase stages. A Gardner-Altman
301 estimation plot illustrates the data across three distinct NSC divisions. Error bars indicate one
302 standard deviation, with the gap representing the mean. The bar in the mean difference
303 comparison reflects the bootstrap 95% confidence interval.
304 (C) aPKC is apically enriched at metaphase in Lgl RNAi NSCs. Comparing apical aPKC
305 membrane enrichment at prophase and metaphase in Lgl RNAi expressing NSCs. Gardner-
306 Altman estimation plot as in (B).
307 (D) Lgl is required to remove aPKC from the basal membrane at metaphase. Comparison of
308 basal aPKC membrane enrichment during metaphase in NSCs expressing Lgl RNAi versus
309 those not expressing it. Gardner-Altman estimation plot as in (B).
310 (E) Lgl is not required for metaphase aPKC polarity. The ratio of apical-to-cytoplasmic aPKC to
311 basal-to-cytoplasmic aPKC during metaphase is depicted for three distinct NSC divisions.
312 Error bars indicate one standard deviation, with the gap representing the mean value.
313 (F) Polarity reset model for Lgl function in NSC asymmetric division. Lgl plays a crucial role in
314 early interphase by removing the Par complex from the membrane, thereby establishing a
315 cleared state essential for resetting polarity. The importance of clearing the Par complex from
316 the membrane during each cell cycle is particularly evident in mitosis. Starting mitosis in a
317 cleared state ensures that the Par complex binds exclusively to the apical membrane through
318 its apical targeting mechanisms. As a result, the fate determinants can effectively polarize to
319 the basal membrane without interference from the Par complex. Without Lgl, the Par complex

persists on the membrane throughout interphase. During early mitosis, the Par complex accumulates at the apical membrane, similar to what occurs in wild-type NSCs, resulting in a polarized distribution. However, in this scenario, residual Par complex remains on the basal membrane during mitosis, effectively preventing fate determinants from binding to the basal membrane as they normally would.

Resource Availability

Lead Contact

Contact the Lead Contact, Kenneth Prehoda (prehoda@uoregon.edu), for further information or to request resources and reagents.

Materials Availability

No new reagents were generated in this study.

Data and Code Availability

Raw data available from the corresponding author on request.

Experimental Model and Subject Details

Fly Strains

Tissue-specific expression of UAS controlled transgenes in NSCs was achieved using a Worniu-GAL4 driver line[33]. Lgl dynamics were imaged using UAS-Lgl-GFP or UAS-Lgl-mCherry (as noted in figure and video legends). Plasma membrane dynamics were imaged using the membrane marker UAS-PLCδ-PH-mCherry, which expresses the pleckstrin homology domain of human PLCδ tagged with mCherry and binds to the plasma membrane lipid phosphoinositide $PI(4,5)P_2$. Chromosome dynamics were monitored using the marker His2A-RFP. Imaging of aPKC was achieved using a BAC-encoded aPKC-GFP[34]. Worniu-GAL4 was used to express UAS-RNAi against aPKC and Lgl in NSCs. Knockdown was enhanced through the co-expression of UAS-Dicer2.

Method Details

Live Imaging

Third instar larvae were incubated at 29ºC for at least 48 hours prior to imaging and dissection. Larvae were dissected in Schneider's Insect Media (SIM) to obtain intact central nervous system explants, which were then mounted on a sterile poly-D-lysine coated 35mm glass bottom dish (ibidi Cat#81156) containing modified minimal hemolymph-like solution (HL3.1). Larval brain explants were imaged using a Nikon Eclipse Ti-2 Yokogawa CSU-W1 SoRa spinning disk microscope with dual Photometrics Prime BSI sCMOS cameras, utilizing a 60x water immersion objective. GFP-tagged proteins were visualized using 488 nm illumination, while RFP and mCherry tags were visualized using 561 nm illumination. Super-resolution

358 images were captured via SoRa (super-resolution through optical photon reassignment)
359 optics[35]. NSCs were identified based on size, location within the central nervous system, and
360 expression of Worniu-GAL4 driven transgenes.
361
362 To acquire "dissociated NSCs", *Drosophila* central nervous systems were collected from third
363 instar larvae and incubated for 30 min at 30°C in Schneider's Insect Medium containing 1
364 mg/mL Papain and 1 mg/mL Collagenase. After incubation, mechanical dissociation was
365 performed by flushing medium/brains through a pipette tip. The resulting cell suspension was
366 then pelleted using gentle centrifugation and washed 3 times with culture medium consisting of
367 Schneider's Insect Medium containing 10% synthetic fetal bovine serum, 20 mM Glutamine,
368 0.05 mg/mL Glutathione, and 0.01 mg/mL Insulin. After the final wash step, cells were
369 resuspended and plated in culture medium consisting of Schneider's Insect Medium containing
370 10% synthetic fetal bovine serum, 20 mM Glutamine, 0.05 mg/mL Glutathione, and 0.01 mg/mL
371 Insulin and imaged with a Nikon Eclipse Ti-2 Yokogawa CSU-W1 SoRa spinning disk
372 microscope with dual Photometrics Prime BSI sCMOS cameras, using a 60x water immersion
373 objective.
374
375 **Pharmacological Inhibition**
376
377 The selective Aurora A inhibitor MLN8237 (Alisertib) was solubilized in DMSO and used at a
378 working concentration of 15 μm in all relevant experiments.
379
380 **Image Processing and Analysis**
381 Imaging data was processed using ImageJ (FIJI package). To correct for photobleaching, the
382 bleach correction tool was used.
383
384 Quantification for Fig. 1D: To quantify the dynamics underlying Lgl's removal from the plasma
385 membrane during early mitosis in NSCs within intact central nervous systems, we used ImageJ
386 to acquire membrane:cytoplasmic ratios for Lgl-GFP signal intensity. To do this, we first
387 measured Lgl membrane intensity by drawing a line with a 5 pixel width perpendicular to the
388 membrane traversing from outside the NSC into the cytoplasm at two different locations, the
389 apical pole and lateral membrane. Lgl membrane signal was quantified using the peak signal
390 intensity along the line. Lgl cytoplasmic signal intensity was measured by taking the average
391 signal intensity within a square ROI (region of interest) drawn inside the NSC cytoplasm, being
392 careful to avoid sampling the nuclear compartment. These measurements allowed us to
393 compare the apical membrane:cytoplasmic ratios to the lateral membrane:cytoplasmic ratios as
394 NSCs moved through early mitosis. The figure depicts the lateral membrane:cytoplasmic ratio at
395 the frame when the apical membrane:cytoplasmic ratio reached ~1 (i.e. Lgl no longer detectable
396 at the apical pole) for each NSC (n = 10).
397
398 Quantification for Figure 1G:
399 To quantify the dynamics underlying Lgl's removal from the basal plasma membrane, we
400 measured the basal membrane:cytoplasmic ratio for Lgl-GFP signal intensity in dissociated
401 NSCs. Dissociated NSCs provided a clearer view of the basal membrane compared to NSCs
402 within intact central nervous systems, where the basal NSC membrane is obscured by the
403 cluster of progeny cells in this region. The figure depicts the time relative to anaphase onset
404 when the basal membrane:cytoplasmic ratio reached ~1 (i.e. Lgl no longer detectable at the
405 basal pole) for each NSC (n = 3). Anaphase onset was determined by using the chromosome
406 marker His2a-RFP to identify the frame when chromosomes aligned at the metaphase plate

407 began to separate.
408
409 Quantification for Figure 1J:
410 To quantify the dynamics underlying Lgl's rebinding to the plasma membrane during mitotic exit
411 and interphase return, we measured membrane:cytoplasmic ratios for Lgl-GFP signal intensity
412 in dissociated NSCs. Dissociated NSCs provided a clearer view of the basal membrane
413 compared to NSCs within intact central nervous systems, where the basal NSC membrane is
414 obscured by the cluster of progeny cells in this region. During mitotic exit and interphase return,
415 cytokinesis is still underway and the nascent sibling cells remain connected by an intercellular
416 bridge containing the cytokinetic pore[32]. Membrane:cytoplasmic ratios were measured at three
417 different locations along the nascent NSC membrane, near the cytokinetic pore (the most basal
418 point of the nascent NSC membrane), the lateral membrane of the nascent NSC, and at the
419 apical pole of the nascent NSC. These measurements were performed at the end of anaphase
420 (when the 2 sets of chromosomes had finished moving apart), early interphase, and later in
421 interphase.

422 Quantification for Figure 2B: To quantify the effects of aPKC knockdown on Lgl's membrane
423 binding over the course of the cell cycle, apical membrane:cytoplasmic ratios for Lgl-GFP signal
424 intensity were measured (as described in Fig. 1D). Ratios were measured at three different time
425 points in the cell cycle. In all the NSCs we sampled, at 15 minutes before nuclear envelope
426 breakdown (NEB) no NSC had begun the rounding up process that marks mitotic entry. We
427 therefore used 15 minutes prior to NEB as the "interphase" time point. NSCs were in the
428 process of rounding up at 7 minutes prior to NEB, and we therefore used this as the "prophase"
429 time point. We used the frame before anaphase onset as the "metaphase" time point. NSCs
430 expressing aPKC RNAi were compared to control cells not expressing RNAi (wild-type).

431 Quantification for Figure 2D: To quantify the effects of Aurora A inhibition on Lgl's removal from
432 the plasma membrane during early mitosis apical membrane:cytoplasmic ratios for Lgl-GFP
433 signal intensity were measured (as described in Fig. 1D). "Prophase" measurements were
434 taken at 6 minutes and 40 seconds prior to NEB. "Metaphase" measurement were taken at 20
435 seconds prior to anaphase onset. NSCs treated with the Aurora A inhibitor solubilized in DMSO
436 were compared to control cells treated with DMSO alone.

437 Quantifications for Figure 3B and 3C: To determine if Lgl's removal from the apical membrane is
438 spatially and temporally correlated with the recruitment of aPKC to the apical membrane during
439 mitotic entry, we used NSCs expressing Lgl-mCherry and aPKC-GFP (n = 3) to measure the
440 lateral and apical membrane:cytoplasmic ratio for both aPKC and Lgl at the frame in which
441 apical Lgl-mCherry signal reached the limit of detection (Lgl membrane:cytoplasmic ratio ~ 1).
442 Figure 3B depicts the lateral and apical membrane:cytoplasmic ratio of Lgl-mCherry signal
443 intensity. Figure 3C depicts the lateral and apical membrane:cytoplasmic ratio of aPKC-GFP
444 signal intensity.

445 Quantifications for Figure 3E and 3F: To determine if the removal of aPKC from the membrane
446 is spatially and temporally correlated with the recruitment of Lgl to the membrane, we performed
447 dual imaging of NSCs expressing Lgl-mCherry and aPKC-GFP (n = 5). The quantifications
448 depict measurements taken during mitotic exit, at the frame in which aPKC-GFP signal near the
449 cytokinetic pore of the nascent NSC reached the limit of detection (membrane:cytoplasmic ratio
450 ~1). Figure 3E compares the membrane:cytoplasmic ratio of Lgl-mCherry signal intensity at two

451 different locations on the nascent NSC, at the basal membrane of the nascent NSC (near the
452 cytokinetic pore) and the lateral membrane. Figure 3F compares the membrane:cytoplasmic
453 ratio of aPKC-GFP signal intensity at two different locations on the nascent NSC, at the basal
454 membrane of the nascent NSC (near the cytokinetic pore) and the lateral membrane.

455 Quantification for Figure 4B: To quantify the effects of Lgl knockdown on aPKC localization at
456 the apical membrane, apical membrane:cytoplasmic ratios for aPKC-GFP signal intensity were
457 measured at interphase (15 minutes prior to NEB), prophase (7 minutes prior to NEB), and
458 metaphase (1 minute before anaphase onset). NSCs expressing Lgl-RNAi (n = 3) were
459 compared to wild-type NSCs (n = 3).

460 Quantification for Figure 4C: To quantify the effects of Lgl knockdown on aPKC localization at
461 the basal membrane, basal membrane:cytoplasmic ratios for aPKC-GFP signal intensity were
462 measured at metaphase (1 minute before anaphase onset). NSCs expressing Lgl-RNAi (n = 3)
463 were compared to wild-type NSCs (n = 3).

464 Quantification for Figure 4D: To quantify the effects of Lgl knockdown on the localization of
465 aPKC to the basal membrane, the basal membrane:cytoplasmic ratio for aPKC-GFP signal
466 intensity was measured at metaphase (1 minute before anaphase onset). NSCs expressing Lgl-
467 RNAi (n = 3) and compared to wild-type NSCs (n = 3).

468 Quantification for Figure 4E: To quantify the effects of Lgl knockdown on aPKC polarity, aPKC
469 signal intensity at the apical and basal poles were compared. The apical membrane:cytoplasmic
470 and basal membrane:cytoplasmic ratio for aPKC-GFP signal intensity was measured at
471 metaphase (1 minute before anaphase onset). To calculate the apical:basal ratio, the apical
472 membrane:cytoplasmic ratio was divided by the basal membrane:cytoplasmic ratio. NSCs
473 expressing Lgl-RNAi (n = 3) were compared to wild-type NSCs (n = 3).
474
475 **Statistical Analysis**

476 Gardner-Altman estimation plots and 95% confidence intervals of datasets were prepared using
477 the DABEST package[36]. Statistical details can be found in the relevant figure legends.

478 **Key Resources Table**

REAGENT or RESOURCE	SOURCE	IDENTIFIER
Experimental Model: Fly Strains		
aPKC-GFP	François Schweisguth Lab[34]	
UAS-Lgl-GFP	Jürgen A. Knoblich Lab[20]	
Histone H2a-RFP (His2a-RFP) (chromosome marker)	Bloomington *Drosophila* Stock Center (BDSC)	BDSC Cat# 23650 RRID: BDSC 23650
Worniu-GAL4 (NSC driver line)	Chris Q. Doe Lab	
aPKC-RNAi	Bloomington *Drosophila* Stock Center (BDSC)	BDSC Cat#67204 RRID: BDSC 67204
Lgl-RNAi	Bloomington *Drosophila* Stock Center (BDSC)	BDSC Cat#38989 RRID: BDSC 38989
UAS-Lgl-mCherry	Jürgen A. Knoblich Lab	

UAS-PLCδ-PH-mCherry (membrane marker)	Bloomington *Drosophila* Stock Center (BDSC)	BDSC Cat#51658 RRID: BDSC 51658
Pharmacological Inhibitors		
MLN8237 (Alisertib)	Selleckchem	Cat#S1133

479
480 **Video Legends**

481 **Video 1: Patterned Lgl membrane displacement and reloading during neural stem cell**
482 **(NSC) divisions**

483 *Part 1: Lgl dynamics in NSCs (imaged in intact central nervous systems).* Super-resolution
484 videos of NSCs expressing Lgl-GFP (Lgl) and His2a-RFP (His2a). Time relative to anaphase
485 onset is indicated. 3 medical section videos of dividing NSCs within intact central nervous
486 systems are shown.

487 *Part 2: Lgl dynamics in dissociated NSCs.* Super-resolution videos of dissociated NSCs
488 expressing Lgl-GFP (Lgl) and His2a-RFP (His2a). Time relative to anaphase onset is indicated.
489 3 medial section videos of dividing dissociated NSCs are shown.

490 *Part 3: 3D projections and medial sections of Lgl and membrane dynamics in NSCs.* Super-
491 resolution videos of NSCs expressing Lgl-GFP (Lgl) and the membrane marker PLCδ-PH-
492 mCherry (membrane). Time relative to nuclear envelope breakdown (NEB) is indicated. 3D
493 projections and medial sections are shown for 3 dividing NSCs within intact central nervous
494 systems.

495 **Video 2: The effects of aPKC knockdown and Aurora A inhibition on Lgl dynamics**

496 *Part 1: The effects of aPKC knockdown on Lgl dynamics.* Super-resolution videos of NSCs
497 expressing Lgl-GFP (Lgl) and aPKC RNAi. Time relative to anaphase onset is indicated. Medial
498 sections are shown for 6 dividing NSCs within intact central nervous systems.

499 *Part 2: Lgl dynamics in NSCs (wild-type control).* Super-resolution videos of NSCs expressing
500 Lgl-GFP (Lgl). Time relative to anaphase onset is indicated. Medial sections are shown for 6
501 dividing NSCs within intact central nervous systems.

502 *Part 3: Lgl dynamics in NSCs treated with Aurora A inhibitor.* Super-resolution videos of NSCs
503 expressing Lgl-GFP (Lgl) and His2a-RFP (His2a) and treated with Aurora A inhibitor. Time
504 relative to anaphase onset is indicated. Medial sections are shown for 3 dividing NSCs within
505 intact central nervous systems.

506 *Part 4: Lgl dynamics in NSCs treated with DMSO.* Super-resolution videos of NSCs expressing
507 Lgl-GFP (Lgl) and His2a-RFP (His2a) and treated with DMSO (vehicle control). Time relative to
508 anaphase onset is indicated. Medial sections are shown for 3 dividing NSCs within intact central
509 nervous systems.

510 **Video 3: Dual imaging of Lgl and aPKC dynamics in dividing NSCs**

511 *Part 1: Lgl and aPKC dynamics during mitotic entry.* Super-resolution videos of NSCs
512 expressing aPKC-GFP (aPKC) and Lgl-mCherry (Lgl). Time relative to anaphase onset is
513 indicated. Medial sections are shown for 3 dividing NSCs within intact central nervous systems.

514 *Part 2: Lgl and aPKC dynamics during mitotic exit.* Super-resolution videos of NSCs expressing
515 aPKC-GFP (aPKC) and Lgl-mCherry (Lgl). Time relative to the start of imaging is indicated.
516 Medial sections are shown for 4 dividing NSCs within intact central nervous systems.

517 **Video 4: The effects of Lgl knockdown on aPKC dynamics**

518 *Part 1: aPKC dynamics in NSCs expressing Lgl RNAi.* Super-resolution videos of NSCs
519 expressing aPKC-GFP (aPKC) and Lgl-RNAi. Time relative to anaphase onset is indicated.
520 Medial sections are shown for 3 dividing NSCs within intact central nervous systems.

521 *Part 2: aPKC dynamics in NSCs (wild-type control).* Super-resolution videos of NSCs
522 expressing aPKC-GFP (aPKC). Time relative to anaphase onset is indicated. Medial sections
523 are shown for 3 dividing NSCs within intact central nervous systems.

524 **Acknowledgments**

525 We thank Eurico Morais-de-Sá for helpful discussions, Sarah Siegrist for a detailed dissociated
526 NSC protocol, and Adam Fries for maintaining the microscope used in this study. This work was
527 supported by NIH grants R35GM127092 and K99GM147601.

528 **Author Contributions**

529 B.L., S.E.W., and K.E.P. designed the experiments. B.L. and S.E.W. performed the
530 experiments. B.L., S.E.W., and K.E.P analyzed the data, prepared the figures, and wrote the
531 manuscript.

532 **Declaration of Interests**

533 The authors declare no competing interests.

534 **References**

535 1. Lang, C.F., and Munro, E. (2017). The PAR proteins: from molecular circuits to dynamic self-
536 stabilizing cell polarity. Dev. Camb. Engl. *144*, 3405–3416. https://doi.org/10.1242/dev.139063.

537 2. Sunchu, B., and Cabernard, C. (2020). Principles and mechanisms of asymmetric cell division. Dev.
538 Camb. Engl. *147*, dev167650. https://doi.org/10.1242/dev.167650.

539 3. Buckley, C.E., and St Johnston, D. (2022). Apical-basal polarity and the control of epithelial form and
540 function. Nat. Rev. Mol. Cell Biol. *23*, 559–577. https://doi.org/10.1038/s41580-022-00465-y.

541 4. Prehoda, K.E. (2009). Polarization of Drosophila neuroblasts during asymmetric division. Cold Spring
542 Harb. Perspect. Biol. *1*, a001388. https://doi.org/10.1101/cshperspect.a001388.

543 5. Bell, G.P., Fletcher, G.C., Brain, R., and Thompson, B.J. (2015). Aurora kinases phosphorylate Lgl to
544 induce mitotic spindle orientation in Drosophila epithelia. Curr. Biol. CB *25*, 61–68.
545 https://doi.org/10.1016/j.cub.2014.10.052.

546 6. Venkei, Z.G., and Yamashita, Y.M. (2018). Emerging mechanisms of asymmetric stem cell division. J.
547 Cell Biol. https://doi.org/10.1083/jcb.201807037.

548 7. Carvalho, C.A., Moreira, S., Ventura, G., Sunkel, C.E., and Morais-de-Sá, E. (2015). Aurora A triggers
549 Lgl cortical release during symmetric division to control planar spindle orientation. Curr. Biol. CB *25*,
550 53–60. https://doi.org/10.1016/j.cub.2014.10.053.

551 8. Grifoni, D., Garoia, F., Bellosta, P., Parisi, F., De Biase, D., Collina, G., Strand, D., Cavicchi, S., and
552 Pession, A. (2007). aPKCzeta cortical loading is associated with Lgl cytoplasmic release and tumor
553 growth in Drosophila and human epithelia. Oncogene *26*, 5960–5965.
554 https://doi.org/10.1038/sj.onc.1210389.

555 9. Yamanaka, T., Horikoshi, Y., Izumi, N., Suzuki, A., Mizuno, K., and Ohno, S. (2006). Lgl mediates
556 apical domain disassembly by suppressing the PAR-3-aPKC-PAR-6 complex to orient apical
557 membrane polarity. J. Cell Sci. *119*, 2107–2118. https://doi.org/10.1242/jcs.02938.

558 10. Moreira, S., and Morais-de-Sá, E. (2016). Spatiotemporal phosphoregulation of Lgl: Finding meaning
559 in multiple on/off buttons. Bioarchitecture *6*, 29–38.
560 https://doi.org/10.1080/19490992.2016.1149290.

561 11. Holly, R.W., Jones, K., and Prehoda, K.E. (2020). A Conserved PDZ-Binding Motif in aPKC Interacts
562 with Par-3 and Mediates Cortical Polarity. Curr. Biol. CB *30*, 893-898.e5.
563 https://doi.org/10.1016/j.cub.2019.12.055.

564 12. Atwood, S.X., Chabu, C., Penkert, R.R., Doe, C.Q., and Prehoda, K.E. (2007). Cdc42 acts
565 downstream of Bazooka to regulate neuroblast polarity through Par-6 aPKC. J. Cell Sci. *120*, 3200–
566 3206. https://doi.org/10.1242/jcs.014902.

567 13. Hutterer, A., Betschinger, J., Petronczki, M., and Knoblich, J.A. (2004). Sequential Roles of Cdc42,
568 Par-6, aPKC, and Lgl in the Establishment of Epithelial Polarity during Drosophila Embryogenesis. *6*,
569 845–854. https://doi.org/10.1016/j.devcel.2004.05.003.

570 14. Lee, C.-Y., Robinson, K.J., and Doe, C.Q. (2006). Lgl, Pins and aPKC regulate neuroblast self-
571 renewal versus differentiation. Nature *439*, 594–598. https://doi.org/10.1038/nature04299.

572 15. Bailey, M.J., and Prehoda, K.E. (2015). Establishment of Par-Polarized Cortical Domains via
573 Phosphoregulated Membrane Motifs. Dev. Cell *35*, 199–210.
574 https://doi.org/10.1016/j.devcel.2015.09.016.

575 16. Dong, W., Zhang, X., Liu, W., Chen, Y.-J., Huang, J., Austin, E., Celotto, A.M., Jiang, W.Z.,
576 Palladino, M.J., Jiang, Y., et al. (2015). A conserved polybasic domain mediates plasma membrane
577 targeting of Lgl and its regulation by hypoxia. J. Cell Biol. *211*, 273–286.
578 https://doi.org/10.1083/jcb.201503067.

579 17. Betschinger, J., Mechtler, K., and Knoblich, J.A. (2003). The Par complex directs asymmetric cell
580 division by phosphorylating the cytoskeletal protein Lgl. *422*, 326–330.
581 https://doi.org/10.1038/nature01486.

582 18. Peng, C.Y., Manning, L., Albertson, R., and Doe, C.Q. (2000). The tumour-suppressor genes lgl and
583 dlg regulate basal protein targeting in Drosophila neuroblasts. Nature *408*, 596–600.
584 https://doi.org/10.1038/35046094.

585 19. Ohshiro, T., Yagami, T., Zhang, C., and Matsuzaki, F. (2000). Role of cortical tumour-suppressor
586 proteins in asymmetric division of Drosophila neuroblast. Nature *408*, 593–596.
587 https://doi.org/10.1038/35046087.

588 20. Wirtz-Peitz, F., Nishimura, T., and Knoblich, J.A. (2008). Linking cell cycle to asymmetric division:
589 Aurora-A phosphorylates the Par complex to regulate Numb localization. Cell *135*, 161–173.
590 https://doi.org/10.1016/j.cell.2008.07.049.

591 21. LaFoya, B., and Prehoda, K.E. (2021). Actin-dependent membrane polarization reveals the
592 mechanical nature of the neuroblast polarity cycle. Cell Rep. *35*, 109146.
593 https://doi.org/10.1016/j.celrep.2021.109146.

594 22. LaFoya, B., and Prehoda, K.E. (2023). Consumption of a polarized membrane reservoir drives
595 asymmetric membrane expansion during the unequal divisions of neural stem cells. Dev. Cell,
596 S1534-5807(23)00159-4. https://doi.org/10.1016/j.devcel.2023.04.006.

597 23. Penkert, R.R., LaFoya, B., Moholt-Siebert, L., Vargas, E., Welch, S.E., and Prehoda, K.E. (2024). The
598 Drosophila neuroblast polarity cycle at a glance. J. Cell Sci. *137*, jcs261789.
599 https://doi.org/10.1242/jcs.261789.

600 24. Moreira, S., Osswald, M., Ventura, G., Gonçalves, M., Sunkel, C.E., and Morais-de-Sá, E. (2019).
601 PP1-Mediated Dephosphorylation of Lgl Controls Apical-basal Polarity. Cell Rep. *26*, 293-301.e7.
602 https://doi.org/10.1016/j.celrep.2018.12.060.

603 25. Lee, C.-Y., Andersen, R.O., Cabernard, C., Manning, L., Tran, K.D., Lanskey, M.J., Bashirullah, A.,
604 and Doe, C.Q. (2006). Drosophila Aurora-A kinase inhibits neuroblast self-renewal by regulating
605 aPKC/Numb cortical polarity and spindle orientation. Genes Dev. *20*, 3464–3474.
606 https://doi.org/10.1101/gad.1489406.

607 26. Oon, C.H., and Prehoda, K.E. (2019). Asymmetric recruitment and actin-dependent cortical flows
608 drive the neuroblast polarity cycle. eLife *8*. https://doi.org/10.7554/eLife.45815.

609 27. Oon, C.H., and Prehoda, K.E. (2021). Phases of cortical actomyosin dynamics coupled to the
610 neuroblast polarity cycle. eLife *10*, e66574. https://doi.org/10.7554/eLife.66574.

611 28. Hirata, J., Nakagoshi, H., Nabeshima, Y., and Matsuzaki, F. (1995). Asymmetric segregation of the
612 homeodomain protein Prospero during Drosophila development. Nature *377*, 627–630.
613 https://doi.org/10.1038/377627a0.

614 29. Knoblich, J.A., Jan, L.Y., and Jan, Y.N. (1995). Asymmetric segregation of Numb and Prospero
615 during cell division. Nature *377*, 624–627. https://doi.org/10.1038/377624a0.

616 30. Spana, E.P., and Doe, C.Q. (1995). The prospero transcription factor is asymmetrically localized to
617 the cell cortex during neuroblast mitosis in Drosophila. Dev. Camb. Engl. *121*, 3187–3195.

618 31. Knoblich, J.A. (2010). Asymmetric cell division: recent developments and their implications for
619 tumour biology. Nat. Rev. Mol. Cell Biol. *11*, 849–860. https://doi.org/10.1038/nrm3010.

620 32. LaFoya, B., Penkert, R.R., and Prehoda, K.E. (2024). The cytokinetic midbody mediates asymmetric
621 fate specification at mitotic exit during neural stem cell division. BioRxiv Prepr. Serv. Biol.,
622 2024.08.27.609974. https://doi.org/10.1101/2024.08.27.609974.

623 33. Albertson, R. (2004). Scribble protein domain mapping reveals a multistep localization mechanism
624 and domains necessary for establishing cortical polarity. J. Cell Sci. *117*, 6061–6070.
625 https://doi.org/10.1242/jcs.01525.

626 34. Besson, C., Bernard, F., Corson, F., Rouault, H., Reynaud, E., Keder, A., Mazouni, K., and
627 Schweisguth, F. (2015). Planar Cell Polarity Breaks the Symmetry of PAR Protein Distribution prior to
628 Mitosis in Drosophila Sensory Organ Precursor Cells. Curr. Biol. CB *25*, 1104–1110.
629 https://doi.org/10.1016/j.cub.2015.02.073.

630 35. Azuma, T., and Kei, T. (2015). Super-resolution spinning-disk confocal microscopy using optical
631 photon reassignment. Opt. Express *23*, 15003–15011. https://doi.org/10.1364/OE.23.015003.

632 36. Ho, J., Tumkaya, T., Aryal, S., Choi, H., and Claridge-Chang, A. (2019). Moving beyond P values:
633 data analysis with estimation graphics. Nat. Methods *16*, 565–566. https://doi.org/10.1038/s41592-
634 019-0470-3.

635

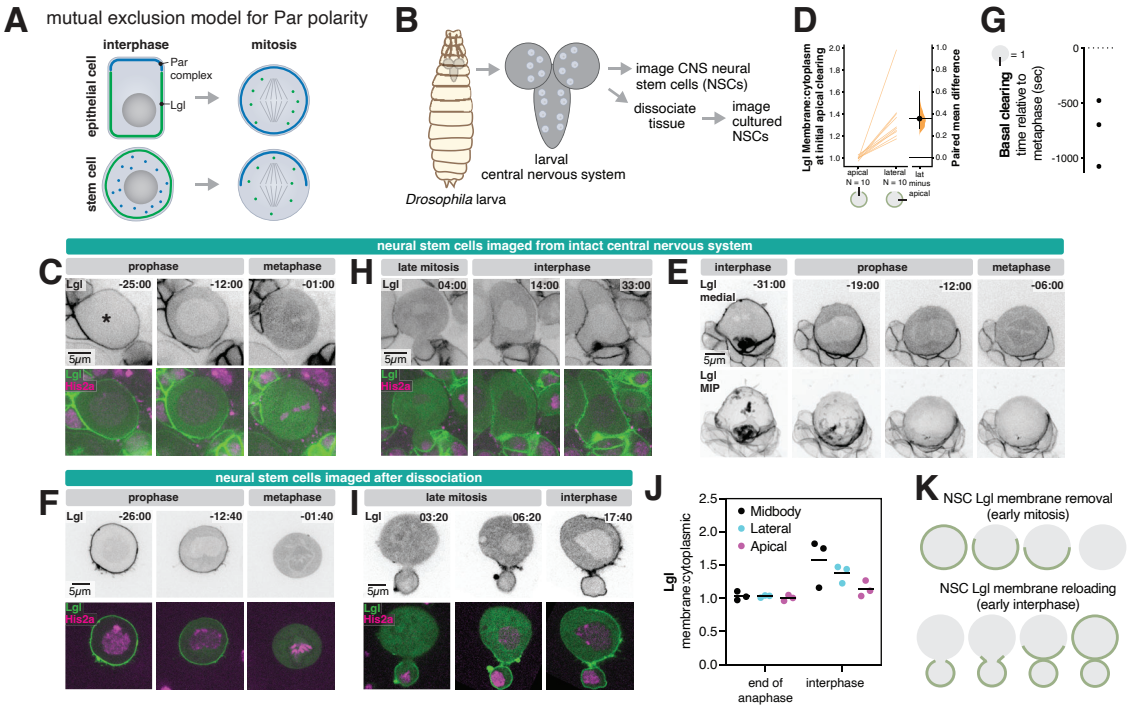
A
mutual exclusion model for Par polarity
interphase
mitosis
epithelial cell
Par complex
Lgl
stem cell
B
image CNS neural stem cells (NSCs)
dissociate tissue
image cultured NSCs
larval central nervous system
Drosophila larva
D
Lgl Membrane:cytoplasm at initial apical clearing
Paired mean difference
apical N = 10
lateral N = 10
lat minus apical
G
= 1
Basal clearing
time relative to metaphase (sec)
0
-500
-1000
neural stem cells imaged from intact central nervous system
C
prophase
metaphase
Lgl
-25:00
-12:00
-01:00
5μm
Lgl His2a
H
late mitosis
interphase
04:00
14:00
33:00
E
interphase
prophase
metaphase
Lgl medial
-31:00
-19:00
-12:00
-06:00
Lgl MIP
neural stem cells imaged after dissociation
F
-26:00
-12:40
-01:40
I
03:20
06:20
17:40
J
Midbody
Lateral
Apical
Lgl membrane:cytoplasmic
2.5
2.0
1.5
1.0
0.5
0.0
end of anaphase
interphase
K
NSC Lgl membrane removal (early mitosis)
NSC Lgl membrane reloading (early interphase)

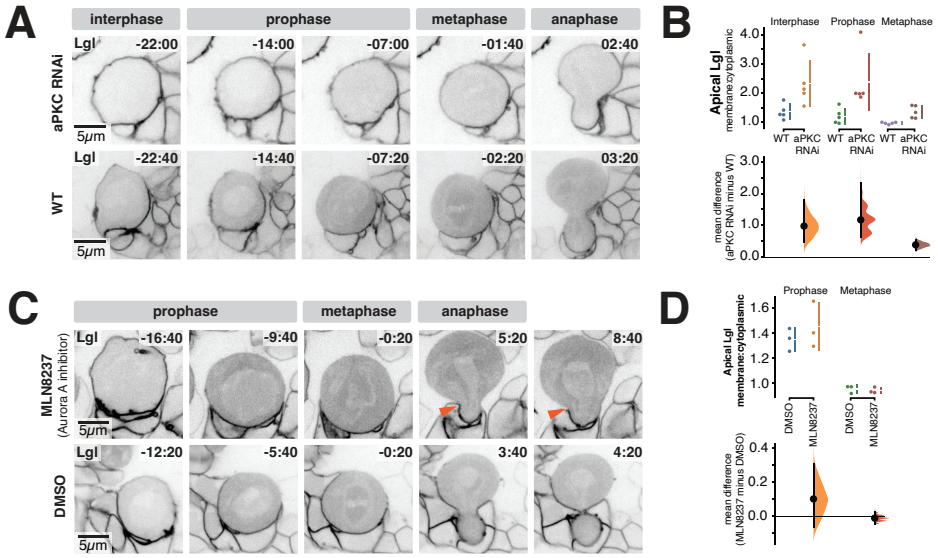
A
interphase
prophase
metaphase
anaphase
aPKC RNAi
Lgl
-22:00
-14:00
-07:00
-01:40
02:40
5μm
WT
Lgl
-22:40
-14:40
-07:20
-02:20
03:20
5μm
B
Interphase
Prophase
Metaphase
Apical Lgl
membrane:cytoplasmic
4.0
3.0
2.0
1.0
WT
aPKC RNAi
WT
aPKC RNAi
WT
aPKC RNAi
mean difference
(aPKC RNAi minus WT)
3.0
2.0
1.0
0.0
C
prophase
metaphase
anaphase
MLN8237
(Aurora A inhibitor)
Lgl
-16:40
-9:40
-0:20
5:20
8:40
5μm
DMSO
Lgl
-12:20
-5:40
-0:20
3:40
4:20
5μm
D
Prophase
Metaphase
Apical Lgl
membrane:cytoplasmic
1.6
1.4
1.2
1.0
DMSO
MLN8237
DMSO
MLN8237
mean difference
(MLN8237 minus DMSO)
0.4
0.2
0.0

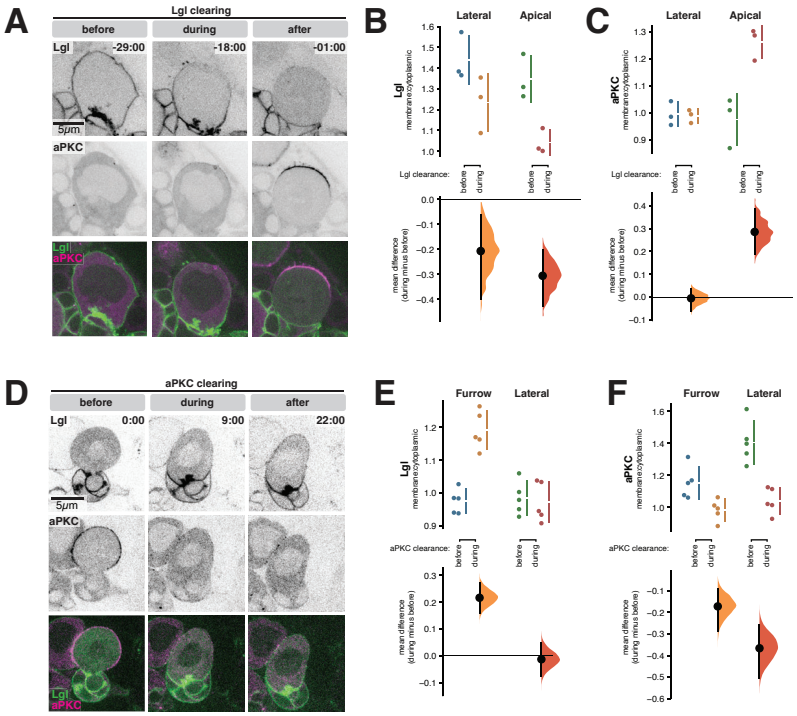
A
Lgl clearing
before
during
after
Lgl
-29:00
-18:00
-01:00
5μm
aPKC
Lgl
aPKC
B
Lateral
Apical
Lgl
membrane/cytoplasmic
Lgl clearance:
before
during
before
during
mean difference
(during minus before)
C
Lateral
Apical
aPKC
membrane/cytoplasmic
Lgl clearance:
before
during
before
during
mean difference
(during minus before)
D
aPKC clearing
before
during
after
Lgl
0:00
9:00
22:00
5μm
aPKC
Lgl
aPKC
E
Furrow
Lateral
Lgl
membrane/cytoplasmic
aPKC clearance:
before
during
before
during
mean difference
(during minus before)
F
Furrow
Lateral
aPKC
membrane/cytoplasmic
aPKC clearance:
before
during
before
during
mean difference
(during minus before)

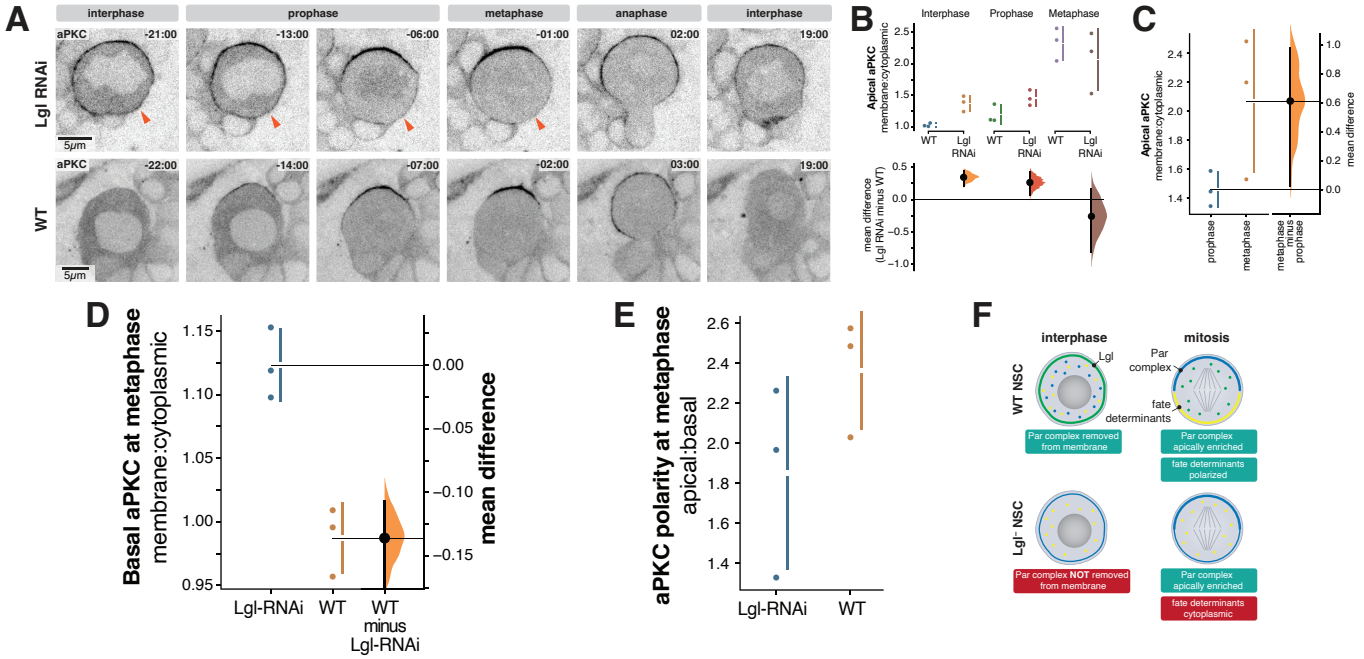
A
interphase
prophase
metaphase
anaphase
interphase
aPKC
Lgl RNAi
WT
5μm
B
Interphase
Prophase
Metaphase
Apical aPKC
membrane:cytoplasmic
WT
Lgl RNAi
mean difference (Lgl RNAi minus WT)
C
Apical aPKC
membrane:cytoplasmic
mean difference
prophase
metaphase
metaphase minus prophase
D
Basal aPKC at metaphase
membrane:cytoplasmic
mean difference
Lgl-RNAi
WT
WT minus Lgl-RNAi
E
aPKC polarity at metaphase
apical:basal
Lgl-RNAi
WT
F
interphase
mitosis
WT NSC
Lgl⁻ NSC
Lgl
Par complex
fate determinants
Par complex removed from membrane
Par complex apically enriched
fate determinants polarized
Par complex NOT removed from membrane
Par complex apically enriched
fate determinants cytoplasmic